

Inlet Flow Separation Control via Novel Lip-Spoilers for Ducted Fan Based VTOL Uninhabited Aerial Vehicles

Cengiz Camci^{1*} Nicholas Herwig² and Ali Aktürk³



ISROMAC 2016

International
Symposium on
Transport
Phenomena and
Dynamics of
Rotating Machinery
Hawaii, Honolulu
April 10-15, 2016

Abstract

The ducted fan propulsion systems provide attractive solutions for manned and unmanned aerial vehicles, with potential applications in general aviation and military missions. They provide higher power-to-thrust ratios over their free-rotor counterpart. However, ducted fans currently implemented in vertical takeoff and landing (VTOL) type aerial vehicles have an inherent duct lip separation and inlet flow distortion problem in edgewise flight. This problem is severe when the flight direction of the VTOL vehicle and the rotor axis of rotation are normal to each other. Separation at the leading edge duct lip for this high angle of attack situation disallows flow from effectively entering the fan rotor causing unwanted inlet flow distortion. Discussed here will be optimized design solutions to controlling and/or eliminating this flow separation at the leading edge duct lip. The designed were three types of lip-s: parametric, detached duct lip, and double duct. The parametric lip-spoilers consisted of inner-face and outer-face duct lip-spoilers. Inner-face duct lip-spoilers predominantly contributed to increased control over the negative nose-up pitching moment while the outer face and detached duct lip-spoilers predominantly controlled the increase in the mass flow rate through the ducted fan rotor. The double-ducted fan (DDF) was successful in eliminating duct lip separation through its added second duct. The main purpose of this study is to design and test various duct lip-spoilers that improves the ducted fan aerodynamic performance in edgewise flight. The conceptual design, analysis and flow visualization for a number of novel lip-spoilers are discussed in detail.

Keywords

VTOL-UAV, ducted fans, inlet flow distortion, lip spoilers, flow control

¹ Prof. of Aerospace Engineering, Dept. of Aerospace Eng., Pennsylvania State University, USA

² currently, research Engineer at Belcan Engineering, Cincinnati, Ohio, USA

³ currently, research Engineer at Siemens Energy, Orlando, Florida, USA

*Corresponding author: cxc11@psu.edu

INTRODUCTION

Ducted fan technologies utilized in piloted or uninhabited vertical takeoff and landing (VTOL) aerial vehicles provide solutions to otherwise complicated applications in general aviation and military operations. What ducted fans provide over their free-rotor counterparts are impact protection for the blades, improved personnel safety, aero-acoustic signature reduction and a higher thrust to power ratio. This increase in the thrust to power ratio is due to the controlled diffusion of the fan rotor jet stream.

Despite providing high performance attributes in many VTOL applications, ducted fans are not without their unresolved problems associated with them, especially in edgewise flight. When in edgewise flight, VTOL ducted

fans encounter flow separation at the leading edge of the duct lip due to a high angle of attack flow condition relative to the inlet plane of the duct. The angle between the inlet flow direction and the axis of rotation of the VTOL lift fan rotor is approximately 90-degrees when in edgewise flight when the duct is stationary with respect to the vehicle.

Studies into the inlet flow characteristics of ducted fans have been of significant interest in the field of uninhabited aerial vehicles (UAVs). Small scale UAV's provide a means of studying lip-separation and the mechanisms of pitching moment generation without endangering personnel or expensing a large portion of funds and time that full scale operational models require. What makes these ducted fan UAV's unique is that they are easily comparable to a large scale ducted fan

vehicle, thus allowing the use of small scale test data to predict large scale vehicle performance.

Graf and Fleming [1] studied lip-spoilers and duct defectors. The lip-spoiler as shown in Figure 1 was applied to the leading edge along a 90-degree arc. They determined that the duct with a lip-spoiler performed better than a duct without it due to the lip-spoiler's ability of reducing the severity of flow separation at the duct lip. The duct deflector on the other hand, outperformed the lip-spoiler at lower angles of attack due to the additional

can provide a significant reduction in pitch-up moment generation, improved thrust/attitude control and reduce the control vane deflections required for vehicle trim across the complete flight envelope.

Akturk and Camci [3] established the principle of a double-ducted fan (DDF) as an inlet lip separation control device. The second duct as shown in Figure 3.b enshrouded the inner duct with a circumferential angle of 360-degrees. Their results showed that a major reduction of the highly 3D and re-circulatory inlet lip

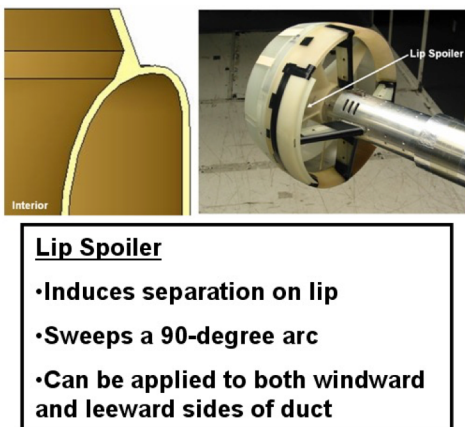


Figure 1. Conventional lip-spoiler as duct lip mounted control effector, Graf and Fleming [1]

drag and reduction in lift it generates. Fleming and Jones et al. [2] investigated the design and analysis of auxiliary control effectors for VTOL UAV's, with the goal of improving performance in crosswind gusts. Understanding the previous investigations on pitching moment, Fleming and Jones studied fourteen variations of auxiliary control effectors and deflectors on a 10-inch ducted fan. It was concluded that the nose-up pitching moment, a principal issue for operating in turbulence, was due to the local distortion of the duct inflow by the crosswind, which quickly increased the windward duct lips local angle of attack.

The idea behind auxiliary control deflectors, or duct lip treatments, was to modify the pressure distribution around the duct lip. When applied to the leading edge, the working principle is that the low pressure suction region would be reduced and when applied to the trailing edge, a favorable nose-down pitching moment would be introduced through adding additional lift. These devices were not effective in zero crosswinds. Their primary design philosophy was to deflect flow and control lip separation when crosswind conditions existed. Ultimately, they concluded that auxiliary control devices

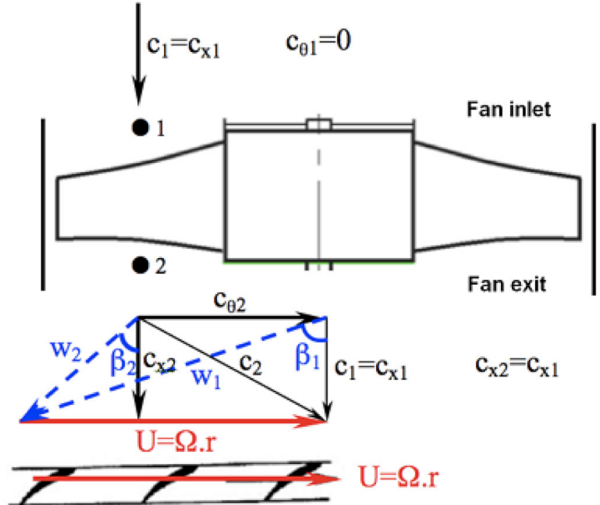


Figure 2. Velocity triangles at the inlet and outlet of the ducted fan rotor, Akturk and Camci [3]

separation zone when the DDF concept is properly implemented. Improved uniformity of fan exit flow and reduced differentials between leading and trailing edges are also other performance enhancing features of this concept. Details of the recently introduced DDF concept by Camci and Akturk are presented in references [4], [5] and [6]. The current study investigates various duct lip control devices, lip-spoilers, attached at varying positions to the leading edge of the duct lip as well as confirming and further optimizing the work of Camci and Akturk's [3] double-ducted fan design (DDF).

COMPUTATIONAL ANALYSIS

A computational analysis was conducted about a 5" ducted fan model for a baseline duct and nine new lip-spoiler design configurations mounted at various positions along the inner and outer faces of the leading edge. Also tested were 5 configurations of a partial double duct design. A three-dimensional computational analysis of the mean flow field around the ducted fan and solutions to the Reynolds Averaged Navier-Stokes

equations (RANS) was performed using the general purpose fluid dynamics solver ANSYS-FLUENT. The rotor flow was effectively simulated using an actuator disk representation of the energy addition process in the rotating frame of reference. The magnitudes of velocity vector, flow direction, static pressure, total pressure pitch-up moment and ducted fan thrust were calculated for an edgewise flow condition where the angle of attack is 90°. All configurations were tested in the forward flight regime consisting of a 20 m/s (39 Knots) edgewise velocity. Specific boundary conditions were imposed in the solver for this forward flight condition. The leading side of the domain was assigned as the velocity inlet while the trailing side was assigned as the pressure outlet. The duct and tailcone surfaces were considered as solid walls with no-slip condition. A symmetry boundary condition was assigned to the top, bottom and remaining sides. The fan boundary condition was described by an actuator disk model that represented the ducted fan rotor. A more detailed description of the computational domain is given in publications by Akturk & Camci [3], [4] and [5].

Reference Ducted Fan Definition: The current study involved in supporting the 3D fan flow computations by use of a wind tunnel flow visualisation approach. Details of the lab model of the reference ducted fan is provided in this paragraph. The brushless DC electric motor driving the five blade ducted fan rotor is speed controlled by an electronic speed control (ESC) system. The high efficiency electric motor driving the fan can deliver 1.5 kW power (2.14 HP). The ducted fan unit is manufactured from carbon composite material and has six vanes at the exit of the fan in order to remove some of the swirl existing at the exit of the rotor. A tail cone is used to cover the motor and hide the electrical wiring. The ducted fan has an inner duct diameter of 136 millimeters and a rotor tip diameter of 126 millimeters. Further operational and design details of the laboratory model of the reference ducted fan can be found in references [3], [4] and [5].

Radial Equilibrium Based Rotor Model: A simplified “rotor actuator-disk model,” from Akturk and Camci [3], was used in place of the 3D rotor flow field in the rotating reference frame as it simultaneously utilizes the radial equilibrium equation, energy equation, and the conservation of angular momentum principle across the fan rotor. The radial equilibrium equation is the force balance in the radial direction at a given axial position, balancing the pressure forces in the radial direction with the centrifugal force. The viscous effects in the actuator disk plane were ignored in this simplified model. For areas other than the actuator disk, a k- ϵ turbulence model was utilized.

The change in pressure across the actuator-disk is calculated at each radial position from hub to tip. The

magnitude of the static pressure jump across the rotor and the change in stagnation enthalpy from rotor inlet to outlet are closely related, as this increase from rotor inlet to outlet is the same as the rate of energy provided to the fluid by the rotor per unit mass flow rate of the duct flow. The magnitude of this pressure jump is mainly controlled by the tangential, or swirl, component $c_{\theta 2}$ of the flow velocity at rotor exit and rotor angular velocity, as determined via the conservation of angular momentum principle and energy equation.

The velocity triangles at inlet (1) and outlet (2) of the ducted fan rotor can be seen in Figure 2. In this model, the blade inlet and outlet angles as measured from the axial direction are labeled as β_1 and β_2 respectively. It can be assumed that the internal energy of the inlet e_1 and outlet e_2 are equal as the rotor is not in the compressible flow range since the tip Mach number does not exceed 0.28. One can also assume that the axial component of the absolute velocity vector is conserved from inlet to outlet $c_{x1}=c_{x2}$ as shown in the velocity triangles of Figure 2. The flow is assumed axial at the rotor inlet where $c_1=c_{x1}$. There is no swirl at the rotor inlet, $c_{\theta 1}=0$. The change in stagnation enthalpy in the ducted fan is represented by eqn. 1 where the right hand side of the equation is the rate of work per unit mass flow rate of air passing from the rotor. Eqn. 1 is a simplified version of the energy equation.

$$h_{02} - h_{01} = U(c_{\theta 2} - c_{\theta 1}) \quad (1)$$

$$U = \Omega \cdot r \text{ and } c_{\theta 1} = 0 \quad (2)$$

$$\left(h_2 + \frac{c_2^2}{2} \right) - \left(h_1 + \frac{c_1^2}{2} \right) = U c_{\theta 2} \quad (3)$$

$$\left(e_2 + \frac{p_2}{\rho_2} + \frac{c_2^2}{2} \right) - \left(e_1 + \frac{p_1}{\rho_1} + \frac{c_1^2}{2} \right) = U c_{\theta 2} \quad (4)$$

When $e_1=e_2$ is substituted into eqn. 3 due to incompressibility, the Euler equation results in as shown eqn. 5. The final equation for the static pressure jump, eqn. 7, is then obtained from eqns 5 and 6.

$$(P_{02} - P_{01}) = U c_{\theta 2} \quad (5)$$

$$\left(p_2 + \rho \frac{c_2^2}{2} \right) - \left(p_1 + \rho \frac{c_1^2}{2} \right) = \rho U c_{\theta 2} \quad (6)$$

$$\Delta p = p_2 - p_1 = \rho [U c_{\theta 2} - \frac{1}{2} (c_2^2 - c_1^2)] \quad (7)$$

Eqn. 7 allows enforcing a prescribed pressure jump, p , in a function of density, radial position, rotor angular speed, Ω , rotor outlet swirl velocity, $c_{\theta 2}$, c_1 and c_2 . This equation can be evaluated at each radial position between the rotor hub and tip resulting in the radial distribution of the static pressure jump. Eqn. 7 can be effectively inserted into any RANS based 3D viscous flow computation as a user defined function.

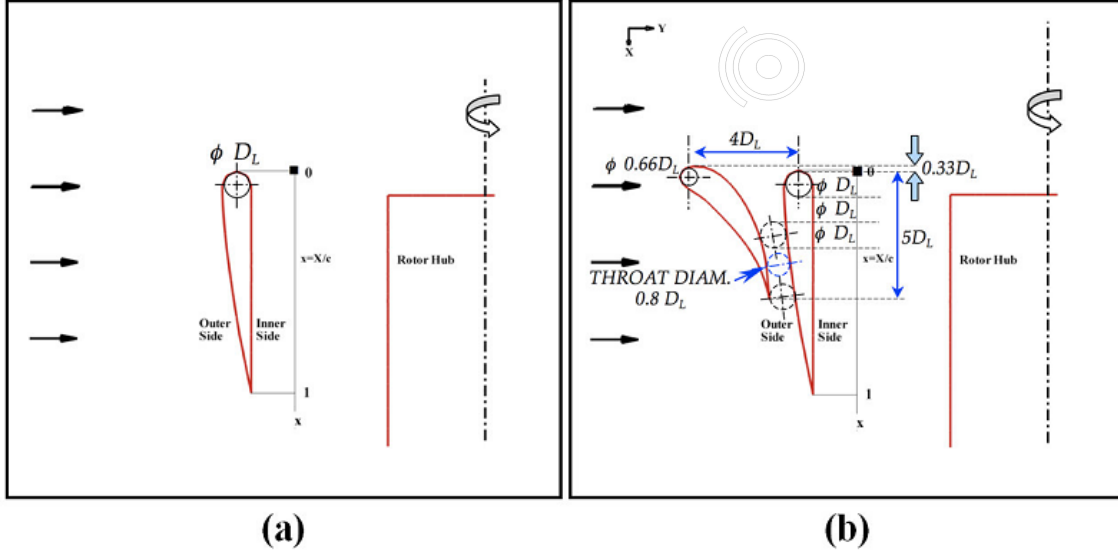


Figure 3. (a) Reference duct airfoil definition in a baseline ducted fan arrangement, (b) Double-Ducted Fan

DESIGN OF LIP-SPOILERS

Parametric Lip-Spoilers: A 5" reference ducted fan configuration briefly described in the previous paragraphs was used to apply the suggested lip-spoiler designs to the inner and outer faces of the leading edge duct lip. Lip-spoilers were defined in terms of circumferential angle θ , spoiler height y , spoiler location with respect to duct lip x , and spoiler angle α . For all configurations a constant $\theta = 120^\circ$ was maintained as shown in Figure 3.c. Table 1 lists x , y , α and θ values for the 6 parametric lip spoiler designs. The positive x

values correspond to locations on the inner face while negative values correspond to locations on the outer duct face. "y" indicates the length of each spoiler in inches. All spoilers have a length of $y=0.3$ inches, except Configuration 5. Design began with the first three lip-spoiler designs attached to the inner duct face. In its following configurations, the lip-spoilers were attached to the outer face at various positions rotating clockwise around the duct lip. Positive α values correspond to the inner-face angle between the spoiler and top of duct lip while negative values correspond to the outer-face angle between the spoiler and top of duct lip. Figure 3.d shows the orientation of the six parametric lip spoilers evaluated in this paper.

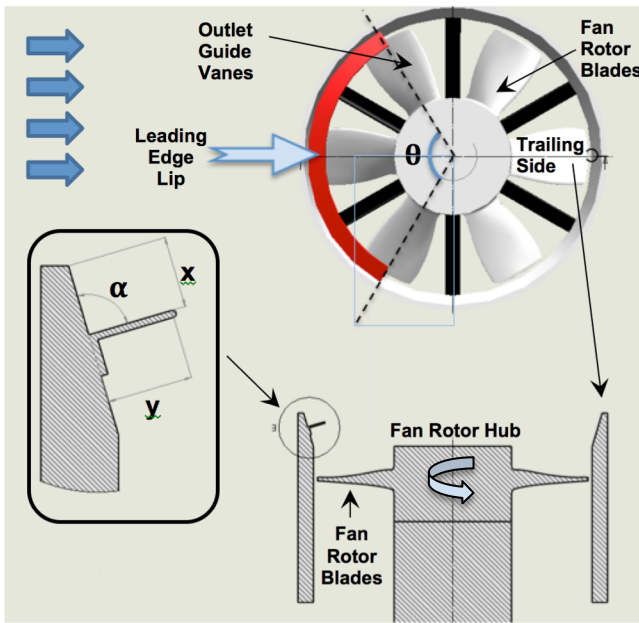


Figure 3.c Parametric geometry definition of lip-spoilers,

	X	y	α	θ
Configuration 1	0.25"	0.30"	+90°	120°
Configuration 2	0.00"	0.30"	+90°	120°
Configuration 3	0.00"	0.30"	0°	120°
Configuration 4	-0.30"	0.30"	-45°	120°
Configuration 5	-0.30"	0.175"	-45°	120°
Configuration 6	-0.30"	0.30"	-50°	120°

Table 1. x , y , α and θ values for the 6 parametric lip-spoiler designs

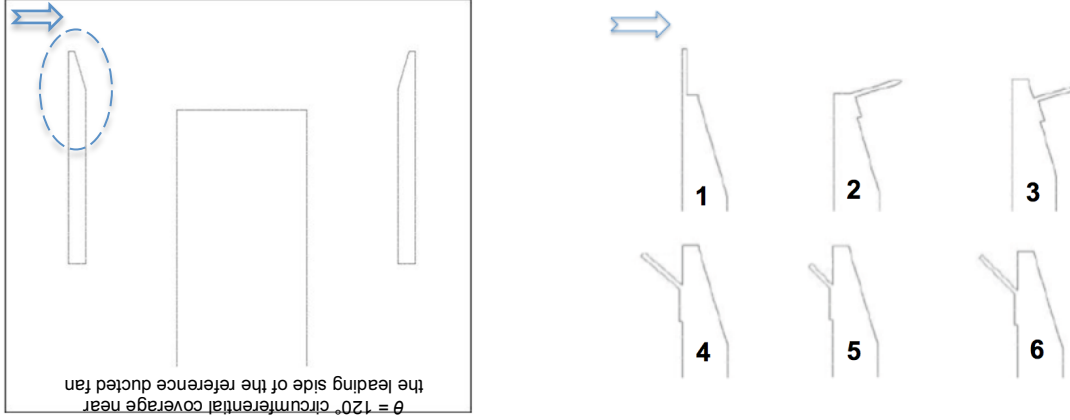


Figure 3.d. Reference ducted fan and the six parametric lip-spoiler designs

Detached Duct Lip-Spoilers: All three of the detached duct lip-spoilers also maintained a circumferential angle of $\theta=120^\circ$ but required a different set of parameters for their geometrical definition. All designs were incorporated into the reference ducted fan as shown in Figure 3.c and 3.d. The governing variable, t_1 , which is the duct wall thickness, establishes the distance between the duct wall and the lip-spoiler, channel thickness, d_1 , as-well-as the thickness, t_2 , of the lip-spoiler itself, as shown in Figure 3.e. The y variable in these configurations corresponds to the spoiler height which is a constant $y=1.13"$ for all three configurations. With the constant duct wall thickness $t_1 = 0.27"$, the lip-spoiler thickness was established to be $t_2 = \frac{2t_1}{3} = 0.18"$. The channel width, d_1 , for Configurations 7,8 and 9 were set equal to the duct wall thickness. The converging channel entrance width, d_2 for Configuration 8 is $d_2 = \frac{3t_1}{2}$. Table 2 shows the overall geometrical

features of all nine configurations including all six parametric lip spoilers and three detached duct lip spoilers.

Partial Double Ducted Fan (PDDF): Due to the double ducted fan's inherent contribution to the nose-up pitching moment, a shape improvement study of the DDF was conducted. Design parameters of the PDDF were adopted from Akturk and Camci [4], [5], [6]. Figure 3.b shows the design characteristics of a typical DDF. The present study focuses on five different configurations with different "partial" second duct coverages, at $\theta = 120^\circ$, 90° , 75° , and 60° . It should be noted that the inner duct for these configurations differs from that of the duct used in conjunction with the lip-spoilers and detached duct lip-spoilers. The double-ducted fan utilizes a smoother, symmetrical airfoil shaped inner duct as shown in Figure 3.b. A list of all five PDDF configurations is given in Table 3.

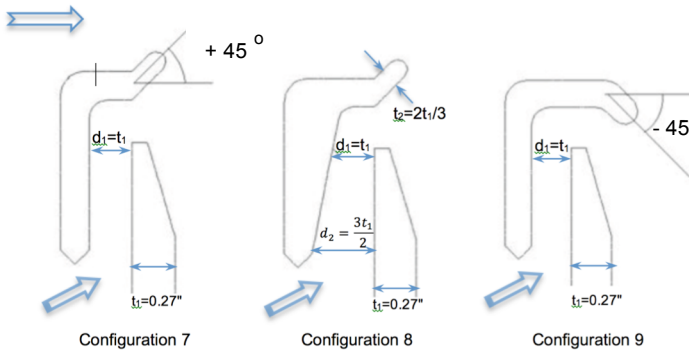


Figure 3.e. Detached Duct Lip-Spoiler designs

Angle	F_T (N)	C_m (N-m)	\dot{m} (kg/s)	C_m/F_T Ratio
Baseline2 (No Duct)	2.294	0.310	0.256	0.135
DDF1 (360 deg)	3.122	0.826	0.290	0.265
DDF2 (120 deg)	2.941	0.703	0.288	0.239
DDF3 (90 deg)	2.925	0.627	0.290	0.214
DDF4 (75 deg)	2.949	0.578	0.289	0.196
DDF5 (60 deg)	2.881	0.516	0.285	0.179

Table 3. All five DDF configurations with five different circumferential coverage angle θ

The governing variable, ΦD_L , which is the leading edge diameter of the inner duct, establishes the width of the throat between the two ducts as $0.8D_L$ at the bottom and

$0.66D_L$ at the top, Figure 3.b. The thrust force F_T , in a ducted fan, in general is calculated from equation 8 when inlet and outlet velocities and mass flow rate through the fan is known.

$$F_T = F_P + \dot{m}(U_e - U_i) \quad (8)$$

The pressure distribution around the duct surfaces, F_P , was also included as duct thrust in calculating the total thrust force. A pitching moment-to-thrust ratio was also calculated as a means to determining which designs were best performing. The pitching moment computation was completed from the post processing of three dimensional RANS results. In this study it is considered that the lower the ratio of pitching moment-to-thrust is, the better the aerodynamic flight performance of the

vehicle. Obtaining increased levels of ducted fan thrust when the pitch up moment generation is minimized is a significant goal of this effort.

EXPERIMENTAL FLOW VISUALIZATION USING A SMOKE-WIRE TECHNIQUE

The smoke-wire setup used in the experiment is very similar to the ones described by Yarusevych [7] and Sieverding [8]. A 0.12 mm diameter, 45 cm long stainless steel wire was attached to the inside of the wind tunnel upstream from the ducted fan model. The wire was coated with a paste of SUDAN dye and mineral oil and heated to the evaporation temperature of the paste, producing a colored smoke for up to 3 seconds

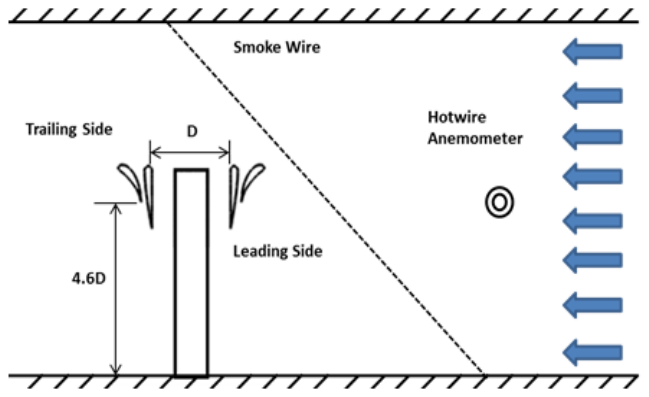
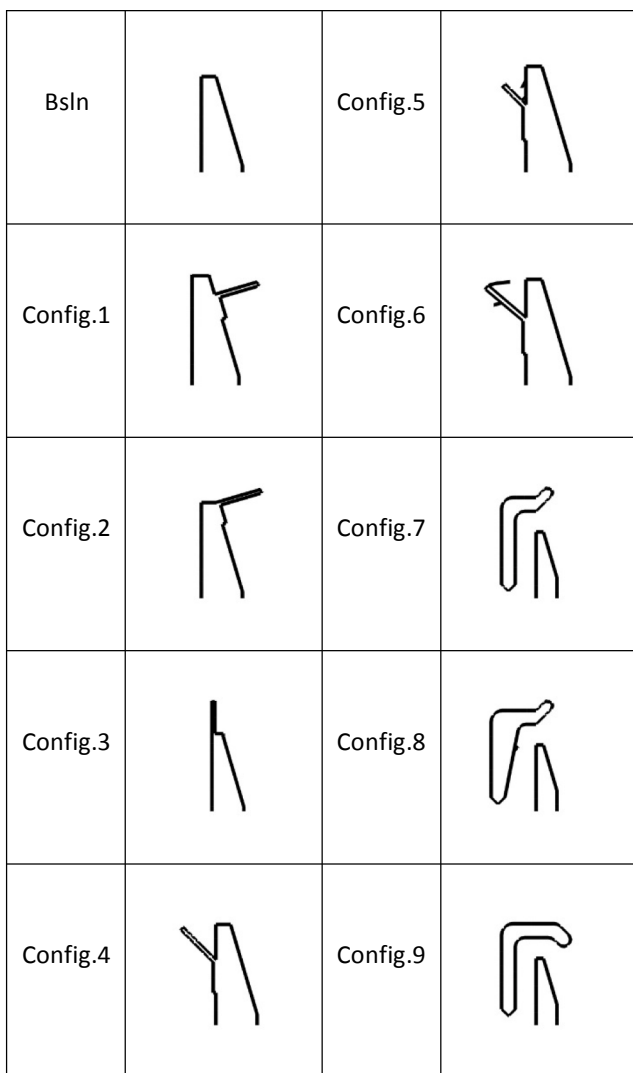


Figure 4. Schematic of flow visualization test setup

in the low wind tunnel speeds of 5 m/s. White light LED strips were used to backlight the visualization region. A Samsung-HD HMX-S16 camera was used for the image acquisition. For best visualization, the camera viewing angle was kept perpendicular to both the wire and the direction of incidence of the light on the field of view. The smoke-wire was located along the centerline axis of the ducted model at a 45° angle measured from the top of the wind tunnel wall above the duct. Flow visualization images were captured at 2 angles; with the first configuration outside the wind tunnel, the camera captured images through the window parallel to the flow-field and the second configuration inside the wind tunnel with the camera downstream of the ducted fan perched 30° above the axis of the fan. A schematic of the test setup is provided in Figure 4. The ducted fan model was attached to the inside of the wind tunnel 4.6D above the bottom surface where D was the diameter of the inner duct. A hotwire anemometer was used to measure crosswind velocities inside the wind tunnel.

Table 2 Overall geometrical features of all nine lip spoiler configurations



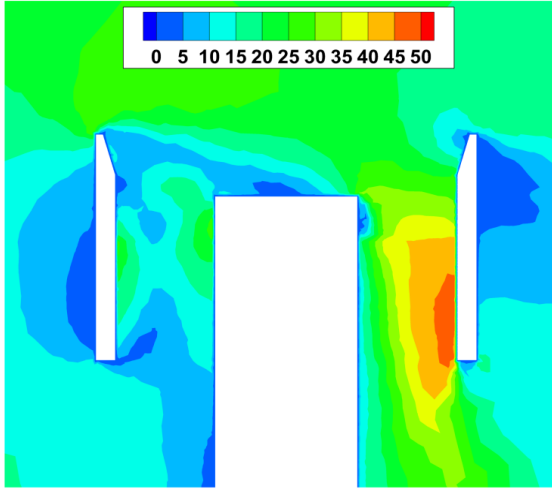


Figure 5. Contours of velocity magnitude (m/s) of Baseline 1

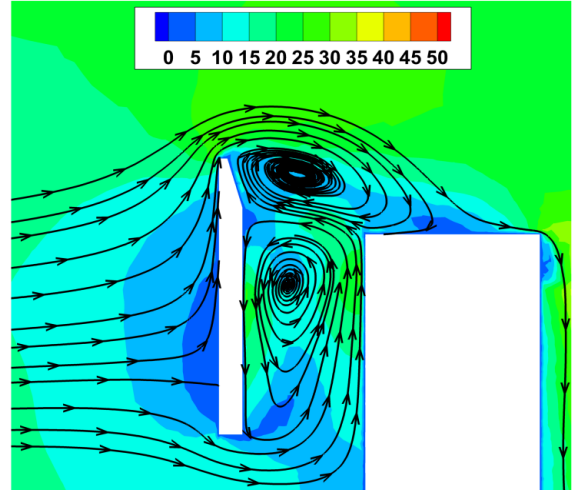


Figure 6. Zoomed view of leading edge Baseline 1 of velocity-magnitude with recirculatory streamlines

RESULTS AND DISCUSSION

Parametric and Detached Duct Lip-Spoilers: All configurations are simulated in the forward flight regime consisting of a 20 m/s (39 Knots) edgewise velocity. Discussed here will be the configurations that displayed significant increases in thrust and control over the nose-up pitching moment. One configuration from each of the designs; inner-face duct lip-spoilers, outer-face duct lip-spoilers, and detached duct lip-spoilers is selected. A nose-up pitching moment-to-thrust ratio, C_m/F_T , was used to obtain the most potentially successful configurations. In general, the inner-face duct lip-spoilers were effective in controlling the nose-up pitching moment over the baseline configuration. This can be attributed to the increase of downward force on the leading edge due to the increased surface area that the inner-face duct lip spoiler creates. Outer-face duct lip-spoilers, in general, were effective in greatly increasing the overall thrust produced by the fan as were the detached duct lip-spoilers over the baseline. The baseline configuration with no lip-spoiler attached had a thrust coefficient, F_T , of 1.655 N, a pitching moment, C_m , of 0.399 N-m and a mass flow rate, \dot{m} , of 0.195 kg/s. It was noticed a great portion of the mass flow entering the duct is localized to the trailing edge of the duct, as seen in the contours of velocity magnitude in Figure 5. It was apparent that little to no airflow was entering near the leading edge of the duct. There is a large, adverse static pressure gradient at the duct lip in the region of severe flow separation. This separation is more apparent in Figure 6, with the addition of streamlines. One can see the separation bubble created above the fan rotor preventing the flow from entering the duct and sending it towards the trailing edge part of the duct. It is this flow that almost impinges on the trailing side duct inner surface that contributes to the (negative)

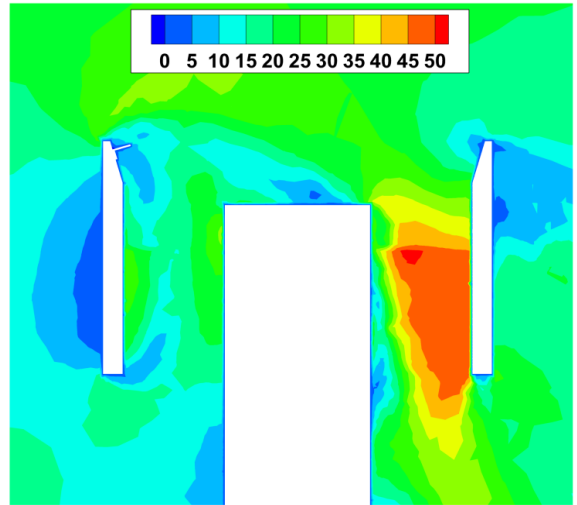


Figure 7. Contours of velocity magnitude (m/s) of Configuration 1

nose-up pitching moment. Also, due to flow impingement near the leading edge region of the duct exterior, some of the relative flow in this area re-enters from the duct exit, further contributing to this (negative) nose-up pitching moment. The three streamlines shown at the bottom part of Figure 6 indicates the re-entry area. The blockage caused by the recirculatory flow features near the leading side of the duct results in a significant flow acceleration on the trailing side of the duct as shown in Figure 5. The rotor energy addition process augments the axial velocity magnitude as indicated by the (red) high speed local flows with a magnitude of about 50 m/s. This velocity magnitude is about 2.5 times the edgewise vehicle speed of 20 m/s. The highly non-uniform duct exit flow for Baseline 1 requires highly complex flow

control surfaces and actuators. It was determined that Configuration 1 performed the best out of the inner-face duct lip-spoilers tested, with a C_m/F_T of 0.193. Overall thrust, F_T , was increased by 9.5%, to 1.812 N, despite

zone, with separation occurring closer to the inner part of the fan. It should be noted that the flow re-entering from the exit section of the duct eventually rises above to

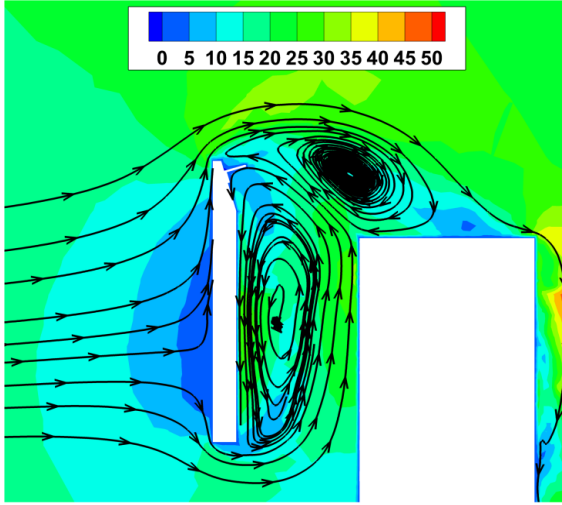


Figure 8. Zoomed view of leading edge Configuration 1 of velocity-magnitude with streamlines.

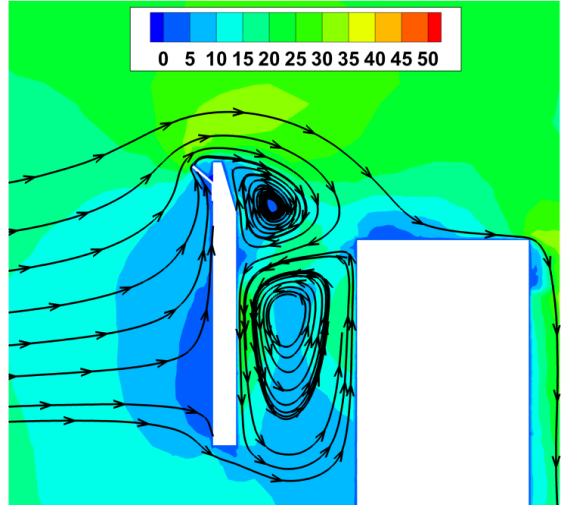


Figure 10. Zoomed view of leading edge Configuration 6 of velocity-magnitude with

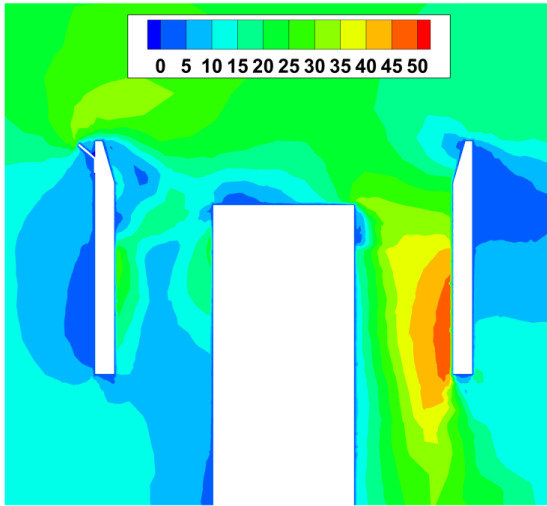


Figure 9. Contours of velocity magnitude (m/s) of Configuration 6.

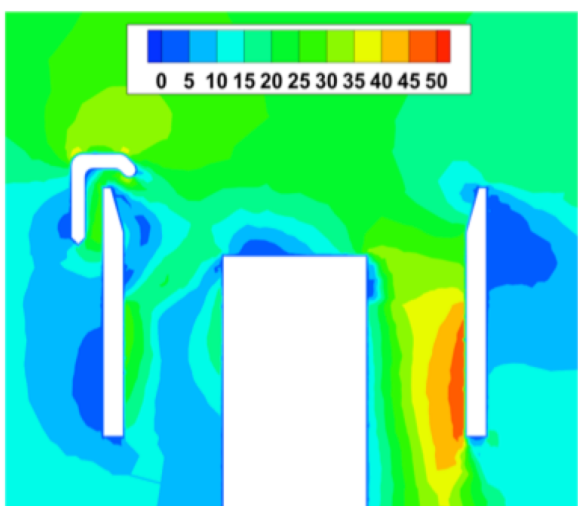


Figure 11. Contours of velocity magnitude (m/s) of Configuration 9.

the mass flow rate, \dot{m} , decreasing by 4%, to 0.187 kg/s. Configuration 1 was highly effective in controlling the (negative) nose-up pitching moment as it was decreased by 13%, to 0.349 N-m, over Baseline 1. When Configuration 1 in Figure 7 is compared to Baseline 1, it did appear that somewhat greater velocities were being experienced near the leading edge duct section. It was surmised that the separation bubble was pushed further towards the inner part of the leading edge of the duct. The streamlines shown in Figure 8 indicate that the inner-face duct lip-spoiler modifies the re-circulatory flow

the level of the lip-spoiler. This occurrence can be attributed to the 4% decay in mass flow rate over baseline. The contour plots are obtained in a vertical plane passing through the leading edge and trailing edge points of the duct. The circumferential flow attributes that are not visible in these contour plots are strong factors for the decay of the final magnitude of the thrust force by 4 %.

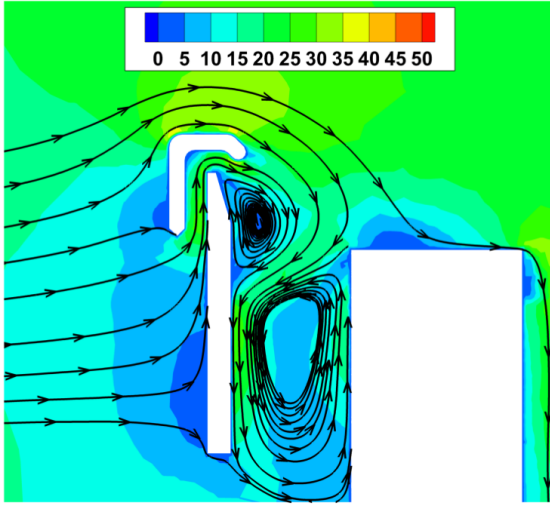


Figure 12. Zoomed view of leading edge Configuration 9 of velocity-magnitude with streamlines.

Configuration 6 performed the best as an outer-edge duct lip-spoiler with a C_m/F_T of 0.181. Overall thrust force F_T was increased by 68%, to 2.778 N, while mass flow rate, \dot{m} , was increased 13%, to 0.221 kg/s. The comparison is with respect to Baseline 1. The recirculatory streamline patterns in Figure 10 shows that the separation bubble was located closer to the leading edge duct lip, thus allowing more air flow to enter the duct and accounting for the 13% and 68% increase in mass flow rate and thrust, respectively. However, with this design, the (negative) nose-up pitching moment was increased by 26%, to 0.503 N-m, over Baseline 1. The lip separation for Configuration 6 occurred closer to the duct lip when compared to Configuration 1. Table 4 provides a list of thrust force F_T , nose-up pitching moment C_m , mass flow rate and C_m/F_T ratio for all nine configurations.

In between all three detached duct lip-spoilers, (Configurations 7,8 and 9) it was concluded from Table 4 that Configuration 9 performed the best with a C_m/F_T value of 0.175. Overall thrust, F_T , was greatly increased over the Baseline by 108%, to 3.456 N, along with mass flow rate, \dot{m} , by 21%, to 0.236 kg/s. However, Configuration 9 resulted in a large increase in nose-up pitching moment which increased by 52%, to 0.605 N-m, over Baseline 1. This increase in nose-up pitching moment is attributed to the increased surface area that the detached duct lip-spoiler adds to the system. Especially the "flow imposed" additional upward force in the small channel between the detached lip-spoiler and the original duct is influential in the nose-up moment augmentation.

It was noticed from Figure 11 that the velocity-magnitude in the duct exit at the trailing edge had slightly decreased over Baseline 1. Figure 12 shows that the entrance

channel of the detached lip guides some of the lip flow effectively into the duct inlet plane on the leading side. The conventional lip separation zone is now pushed towards a larger outer radius. The leading side of the duct breathes air more effectively because of the detached lip Configuration 9. The detached duct lip-spoiler was effective in channeling the leading edge/lip flow into the duct and directing flow downward through the fan. The size of the separation bubble induced by the detached lip is the smallest among these configurations and localized near the duct inner surface thus allowing the flow to enter this region. Also noticed was that a limited amount of flow was entering from the exit plane of the duct on the leading side as compared to Baseline 1 and Configuration 1.

A non-dimensionalized total pressure coefficient C_{po} was used to compare the configurations against one another for their aerodynamic loss characteristics in Figure 13. The light and dark blue regions indicate the major aerodynamic loss areas in the separated flow zones. The yellow and brown areas show the local flow zones where there is a total pressure excess mainly in the rotor downstream region.

The lip separation induces three significant areas in which there are strong total pressure variations. The most significant loss areas are in the lip separation zone near the leading edge and the hub separation zone just downstream of the rotor hub in front of the rotor actuator disk plane. The third area with strong total pressure variation is in the rotor downstream region near the trailing side of the duct. Configuration 6 and 9 reduced the coverage of excess total pressure zone near in the trailing side of the duct. This excess total pressure region downstream of the rotor is inherent to most ducted fans operating at high angle of attack with strong inlet lip separation. Any design that helps to reduce this excess total pressure could be classified as an improved design.

Lip-Spoiler	F_T (N)	C_m (N-m)	\dot{m} (kg/s)	C_m/F_T Ratio
Baseline1 (No LS)	1.655	0.399	0.195	0.241
Configuration 1	1.812	0.349	0.187	0.193
Configuration 2	1.667	0.372	0.191	0.223
Configuration 3	1.770	0.426	0.194	0.241
Configuration 4	2.668	0.500	0.220	0.187
Configuration 5	2.137	0.440	0.207	0.206
Configuration 6	2.778	0.503	0.221	0.181
Configuration 7	2.154	0.406	0.202	0.188
Configuration 8	2.250	0.473	0.204	0.210
Configuration 9	3.456	0.605	0.236	0.175

Table 4. Performance comparison of all nine lip-spoiler configurations evaluated using C_m/F_T

The detached lip-spoiler of Configuration 9 resulted in the smallest recirculatory flow zone affecting the rotor inlet flow in the usual lip separation area. Configuration 6 also has a measurable lip separation reduction when compared to the baseline. The size of the relatively small hub separation region is strongly influenced from the size and strength of the re-circulatory flow in the lip separation area. Configuration 6 and 9 provides the least amount of recirculatory flow in the hub separation region.

In Baseline 1 as shown in Figure 13.a, the separation bubble almost covers the entire leading edge region above the fan rotor as compared to Figures 13.c and 13.d. The outer-edge duct lip spoiler pulls the separation bubble toward the leading edge duct lip allowing for air flow to enter the fan rotor more effectively. The detached lip spoiler of Configuration 9 is also highly effective in reducing the inlet lip separation zone.

[3],[4],[5] and [6]. Figure 3.a and 3.b shows the original design characteristics of a double-ducted fan (DDF). Although the second (outer) duct of the original (DDF) surrounds the inner duct all around the circumference, the partial double-ducted fan (PDDF) uses a partial treatment covering only the frontal part of the vehicle. The present study focuses on four different configurations with different "partial" second duct coverage, at $\theta = 120^\circ, 90^\circ, 75^\circ, \text{ and } 60^\circ$. Table 3 presents the design characteristics of all partial double-ducted fan (PDDF) configurations. The predicted thrust, pitch-up moment, duct mass flow rate values for all (PDDF) configurations are also provided in Table 3.

Baseline 2 had a pitching moment-to-thrust ratio, C_m/F_T , of 0.135, much lower than any of the lip-spoiler configurations. Contours of its velocity magnitude with streamlines are plotted in Figure 15. It was calculated

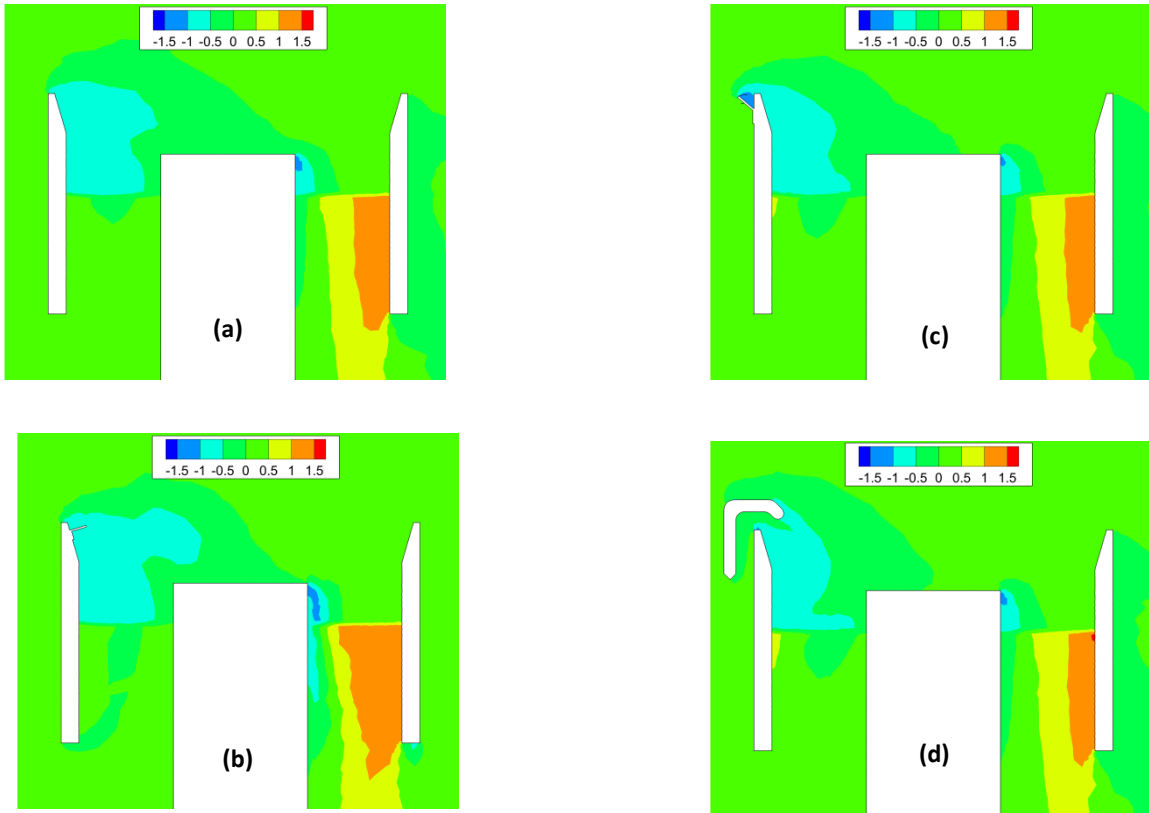


Figure 13. Non-dimensionalized total pressure coefficient of $c_{po} = \frac{(P_o - P_{ref})}{0.5 \cdot \rho \cdot U_i^2}$
(a) Baseline 1, (b) Configuration 1, (c) Configuration 6, (d) Configuration 9

Partial Double Ducted Fan (PDDF): Double-ducted fan configurations utilize a different inlet lip separation control geometry over the lip-spoiler configurations. The inner duct uses a smoother airfoil profile as shown in Figure 14. In order to generate a reference basis, a reference duct named "Baseline 2" was designed as shown in Figure 14. The underlying principles of double-ducted fan design is given by Akturk and Camci

that this set-up called for the inner duct had a mass flow rate, \dot{m} , of 0.256 kg/s, that is 31% greater than Baseline 1 and a pitching moment of 0.310 N-m that is 22% less than Baseline 1. It was also noticed that the double ducted fan configurations displayed a linear downward trend in pitching moment; as the circumferential angle θ of the second duct was reduced from 360° , pitching moment also decreased. In the partial double-ducted

fan configurations thrust, F_T , and mass flow rate, \dot{m} , maintained steady values, suggesting Independency from the circumferential angle of the outer duct. This is due to the fact that, for a selected value of θ , thrust generation is achieved in the inner duct.

In (DDF1), the ducted-fan with $\theta = 360^\circ$ coverage, thrust, F_T , was increased by 36%, to 3.122 N, and the mass flow rate, \dot{m} , was increased by 13% to 0.290 kg/s. Take note to the large increase in the nose-up pitching moment, it is more than two-and-a-half times that of Baseline 2. The added surface area of the second duct is adversely affecting the nose-up pitching moment generation.

The contours of velocity-magnitude in Figure 16 and 17 show that, with the addition of the second duct, flow separation at the duct lip is effectively eliminated. This result also confirms the findings of Akturk and Camci [3]. Flow in DDF 1 freely enters the rotor/actuator disk area of the ducted-fan unit. The exit flow conditions are much more uniform because of the elimination of the rotor inlet flow distortion. Flow separation, minimally, occurs at the trailing edge region of the rotor hub, but appears to not affect overall flow the duct exit region. It was noticed in Figure 17 that the airflow travelling in the (DDF1) inner duct preceeded to the duct exit without any recirculatory flow obstruction. The partial double-ducted fan configurations maintained their high level of thrust and mass flow attributes over Baseline 2. These features are numerically compared in Table 3.

The $\theta=60^\circ$, DDF5, configuration resulted in the lowest nose-up pitching moment, at 0.516 N-m, and pitching moment-to-thrust ratio, at 0.179. The contours of velocity-magnitude are given in Figure 18. Strong similarities to DDF1 were noticed. No significant duct lip separation was noticed at the leading edge and flow travelled through the leading edge of the duct into the exit plane continuously without flow re-entering the exit region from the frontal area of the vehicle.

Overall, DDF5 had a 26% increase in thrust, to 2.881 N, an 11% increase in mass flow rate, to 0.285 kg/s, and a 66% increase in the nose-up pitching moment, to 0.516 N-m, over Baseline 2. However, DDF5 did display a nose-up pitching moment 38% less than the $\theta=360^\circ$ DDF1 while losing less than 8% thrust and 2% mass flow. This observation suggests that with even smaller circumferential θ angles, the partial double ducted fan PDDF should still maintain the high values of thrust and mass flow, with diminished nose-up pitching moment over these configurations discussed here.

The total pressure coefficient C_{po} in Figure 20 was used to compare the configurations against one another for local aerodynamic penalty visualization. Significant leading edge lip separation and enhanced total pressure

impact on the inner part of the aft section of the duct (Baseline 2) is apparent in Figure 20.a. DDF1 and DDF5 provide a measurable reduction of the enhanced total pressure impact on the inner part of the aft section of the duct in Figure 20.c and 20.c. In general, when the severity of the inlet flow distortion or lip separation is reduced, a more uniform total pressure distribution is observed in a ducted fan in the circumferential direction as reported by Akturk and Camci [4], [5], [6].

Flow Visualization: Flow visualization was carried out experimentally for the Baseline 2 and DDF1 configuration where $\theta = 360^\circ$. The computational and analytical models were compared to the visualizations obtained at 6,000 rpm and 5 m/s vehicle edgewise velocity. 5 m/s was selected in order to obtain clear and comparable flow visualizations in the wind tunnel. Separate computational analysis for the current visualisation effort needed to be conducted at 5 m/s in order to obtain comparable streamline patterns. It should be noted that all other computations in this paper were conducted in the forward flight regime consisting of a 20 m/s (39 Knots) edgewise velocity. The results between the computational model and wind tunne flow visualization experiment do agree well with one another.

Figure 21 compares the flow visualization images to the RANS computations for Baseline 2. Flow approaching from the left stagnates against the duct wall and follows upward where it enters the fan leading edge lip region. The lip separation on the inner part of the leading edge area is clearly visible in the computations. These computational observations are fully confirmed by the smoke flow-wire visualization in Figure 21.c.

Figure 22 compares the computations and smoke-wire flow visualizations for DDF1 configuration. Computational results show that the crosswind entered the channel between the inner and outer ducts from the bottom and travelled upward to the inner duct lip area as shown in Figure 22.b. The flow visualization image shown in Figure 22.c confirms the computational result.

Figure 23 displays the computational and flow visualization results for the Baseline2 configuration. The specific orientation of the camera was chosen to enhance the streamline images at the entrance region of "Baseline 2". The lip separation region and the rotor hub separation area is clearly visible in both computation and visualization. Figure 24 is a comparison of computations and visualizations for the DDF1 configuration from a different camera orientation in an effort to enhance the duct inlet flow features. The computed streamline patterns are highly consistent with the visualized ones.

A partial double-ducted fan was computationally investigated using the RANS method described in this

paper. Figure 25 presents the computationally obtained flow features for DDF 5 configuration with a circumferential coverage of $\theta = 60^\circ$. One of the most significant results of this investigation is the finding that the lip separation control feature of a partial double-ducted fan at $\theta = 60^\circ$ is about the same as $\theta = 360^\circ$ double ducted fan. The implementation of a partial second duct provides a significant weight gain in addition to the reduced manufacturing cost of the vehicle. The second duct could even be implemented as a deployable and controllable simple control surface in a flight vehicle.

SUMMARY AND CONCLUSIONS

Reducing the re-circulatory lip separation, improving the thrust and duct mass flow rate and reducing the nose up

pitching moment of a ducted fan system were considered as the most essential aeromechanical performance attributes of an inlet flow distortion reduction system in a VTOL UAV vehicle. Six parametric lip spoilers and three detached lip spoilers along the leading edge of a ducted fan were evaluated in detail for their lip separation control characteristics. The lip-spoilers were characterized as inner-face, outer-face and detached duct lip-spoilers. It was determined that the inner-face duct lip-spoilers were the most effective in controlling the nose-up pitching moment with Configuration 1. The outer-face and detached duct lip-spoilers were the most effective in increasing and controlling the mass flow rate alone through the leading edge of the duct with Configurations 6 and 9 displaying the best abilities at doing so. Also studied were the effects of varying the circumferential angle θ of the outer duct for five different partial double-ducted fans.

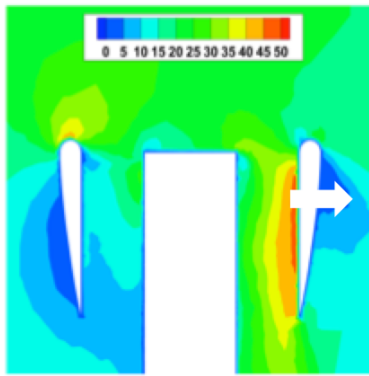


Figure 14. Contours of velocity magnitude (m/s) of Baseline 2.

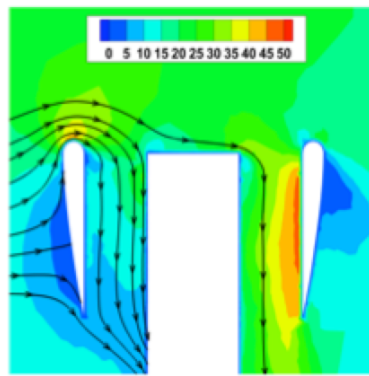


Figure 15. Contours of velocity magnitude (m/s) with streamlines of Baseline 2.

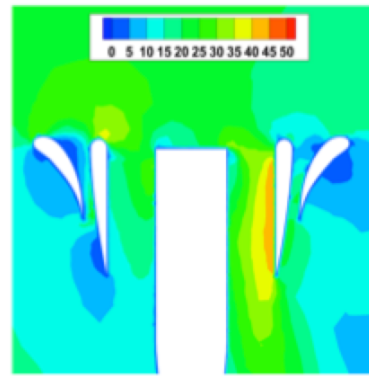


Figure 16. Contours of velocity magnitude (m/s) of DDF 1.

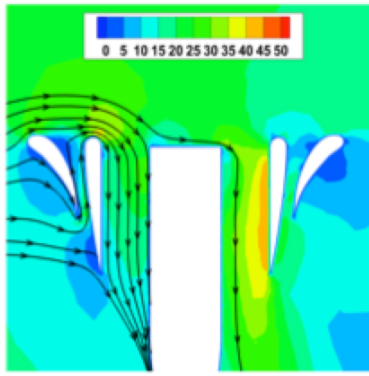


Figure 17. Contours of velocity magnitude (m/s) with streamlines of DDF 1.

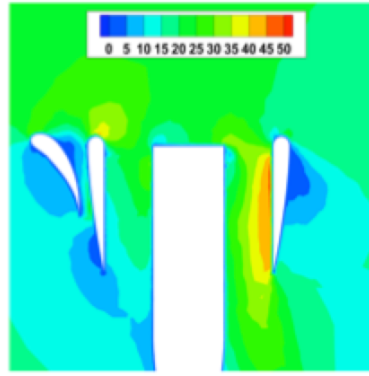


Figure 18. Contours of velocity magnitude (m/s) of DDF 5.

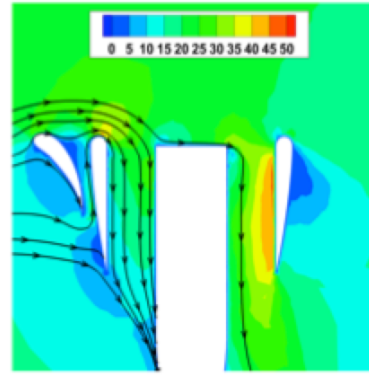


Figure 19. Contours of velocity magnitude (m/s) with streamlines of DDF 5.

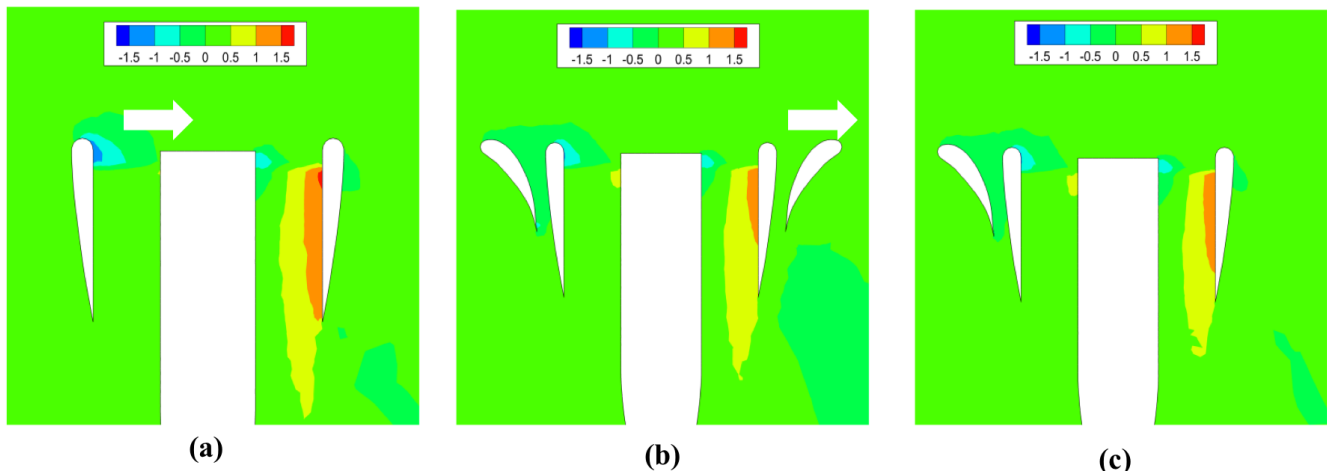


Figure 20. Non-dimensionalized total pressure coefficient of (a) Baseline 2, (b) DDF1, and (c) DDF5.

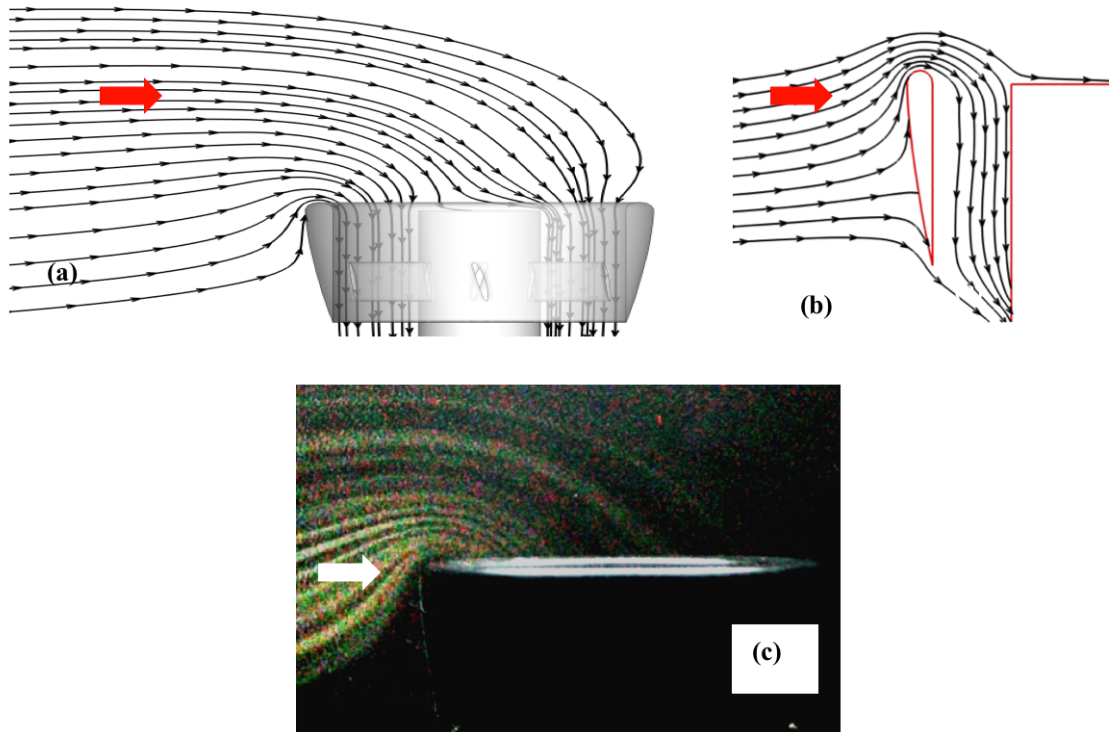


Figure 21. Flow visualization and computational analysis of Baseline 2, (a) side view of computed streamlines, (b) computed inner duct streamlines, (c) smoke-wire flow visualization, at 6,000 rpm and 5 m/s crosswind.

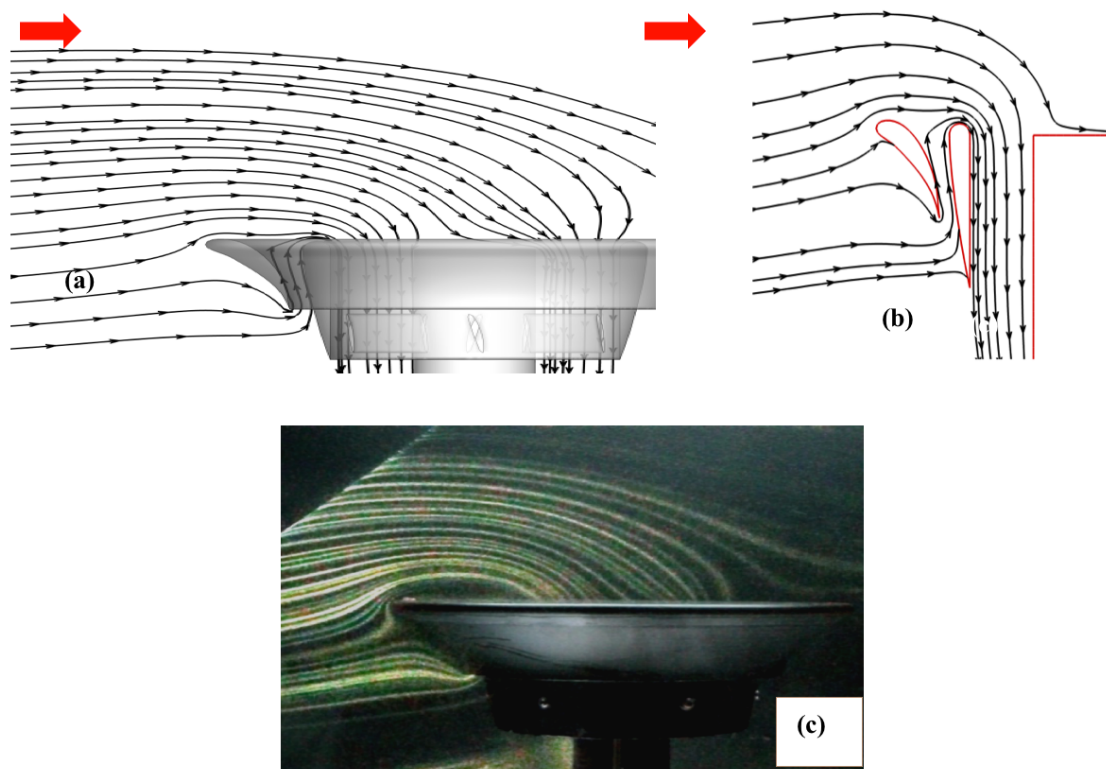


Figure 22. Flow visualization and computational analysis of DDF1, (a) side view of computed streamlines, (b) computed inner duct streamlines, (c) smoke-wire flow visualization, at 6,000 rpm and 5 m/s crosswind.

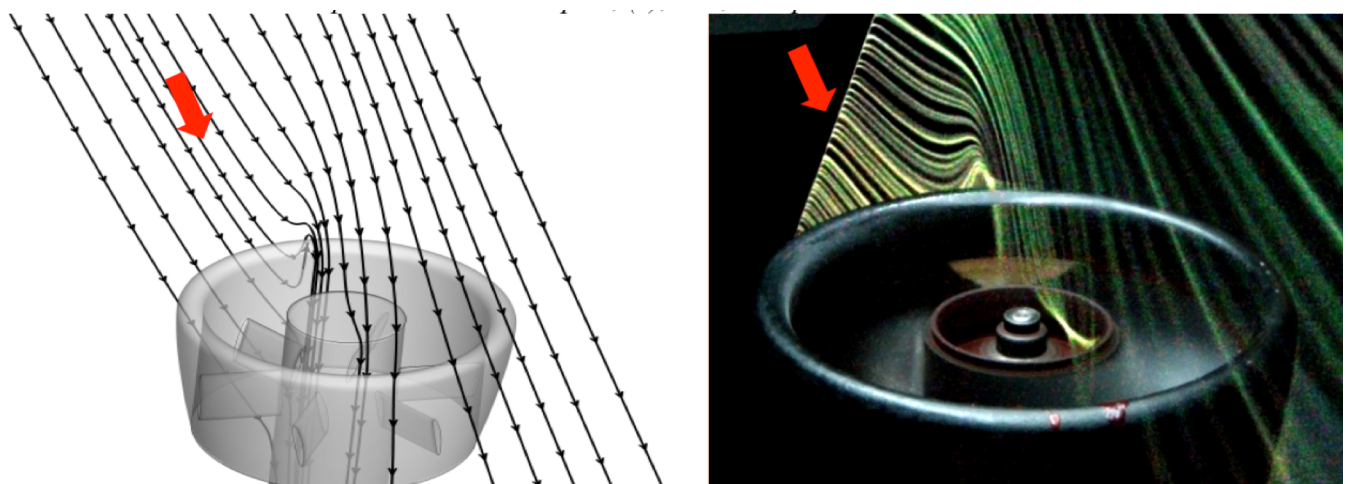


Figure 23. Computational analysis (left) and flow visualization (right) of Baseline 2 at 6000 rpm and 5 m/s crosswind

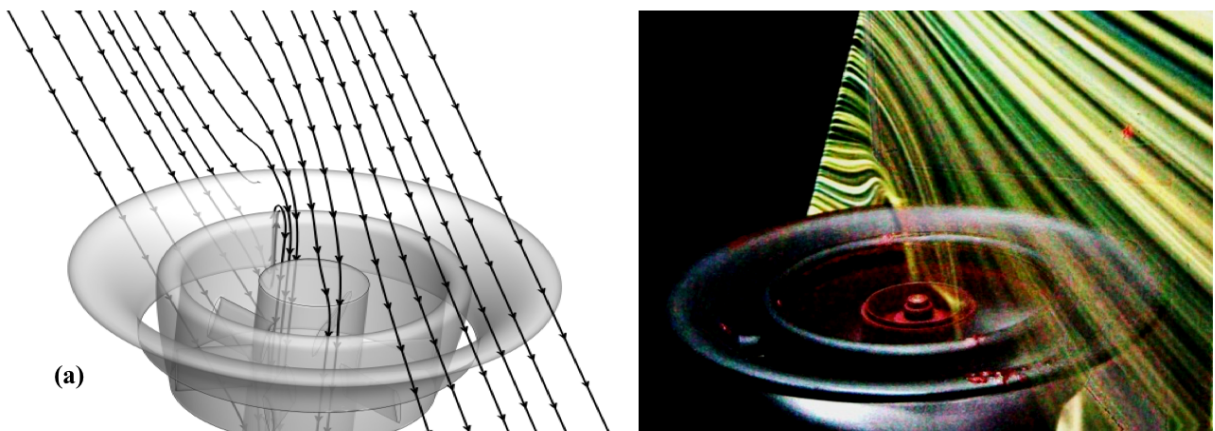


Figure 24. Computational analysis (left) and flow visualization (right) of of DDF1 at 6000 rpm and 5 m/s crosswind, $\theta = 360^\circ$, full Double-Ducted Fan

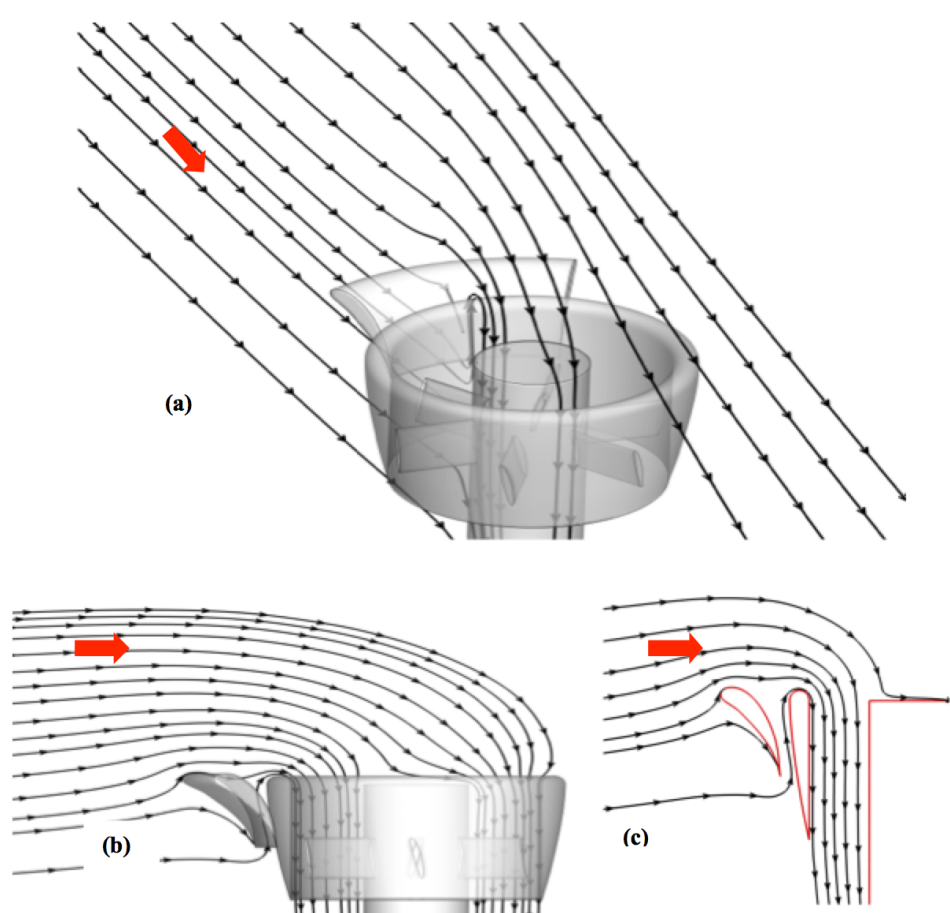


Figure 25. Computationally obtained flow features of DDF5 at 6000 rpm and 5 m/s crosswind, Partial Ducted-Fan, $\theta = 60^\circ$

One of the most significant results of this investigation is the finding that the lip separation control feature of a partial double-ducted fan at $\theta=60^\circ$ is about the same as $\theta=360^\circ$ double ducted fan. The nose-up pitching moment in a (PDDF), consistently decreased with reduced circumferential angle θ . This observation was attributed to the fact that there is less surface area for approaching flow to make contact with.

The implementation of a partial second duct provides a significant weight gain in addition to the reduced manufacturing cost of the vehicle. The second duct could even be implemented as a deployable and controllable simple control surface in a flight vehicle.

Flow visualization of the double-ducted fan concept was then performed in the wind tunnel environment and compared to its computational counterpart. Wind tunnel flow visualization agreed very well with the computational study for all configurations thus proving its abilities in the design of inlet flow reduction systems in VTOL UAV vehicles.

Computational fluid dynamics is a highly effective approach in designing passive flow control systems such as lip spoilers and double-ducted fan systems. Reducing the coverage of the strong re-circulatory flow zones near the leading edge lip of VTOL UAV based ducted fans.

NOMENCLATURE

B_1, B_2	Blade inlet, exit angle measured from axial direction (deg)
c_1, c_2	Rotor inlet, exit absolute velocity (m/s)
C_{po}	Total pressure coeff. $C_{po} = \frac{(P_o - P_{ref})}{0.5 \cdot \rho \cdot U_i^2}$
c_θ	Tangential (swirl) velocity component (m/s)
c_{x1}, c_{x2}	Inlet, outlet axial Component of velocity (m/s)
D_L	Thickness of duct lip entrance (m)
d	Channel width between inner and outer duct (m)
F_p	Pressure forces (pa)
F_T	Thrust force (N)
\dot{m}	Mass flow rate (kg/s)
p	Static pressure (pa)
P_0	Total pressure (pa)
ρ	Density (kg/m ³)
w_1, w_2	Rotor inlet, outlet relative velocity (m/s)
r	Radial distance (m)
t_1	Duct wall thickness (m)
t_2	Lip-spoiler thickness (m)
U_i, U_e	Inlet, outlet velocity (m/s)
θ	Circumferential angle of lip-spoiler (deg)
Ω	Rotational Speed (radians/s)

ACKNOWLEDGMENTS

The authors acknowledge the financial support of the PSU Vertical Lift Center of Excellence (VLRCOE) and the National Rotorcraft Technology Center (NRTC) (Under U.S. Army Research Office Grant No. W911W6-

06-2-0008). They wish to thank Dr. Ozhan Turgut for his support throughout this effort. Cengiz Camci also acknowledges the support provided by TUBITAK, The Scientific and Technological Research Council of Turkey and Istanbul Technical University, during the final editing phase of this paper. Mr.R.Auhl, M.Catalano and K.Hellen of Aerospace Engineering at Penn State provided significant technical expertise in all of our ducted fan related experimental and large scale computing efforts.

REFERENCES

- [1] Graf, W., Fleming, J., and Wing, Ng., "Improving Ducted Fan UAV Aerodynamics in Forward Flight" 46th AIAA Aerospace Sciences Meeting and Exhibit, Reno, Nevada January 2008
- [2] Fleming, J., Jones, T., Lusardi, J., Gelhausen, P., and Enns, D., "Improved Control of Ducted Fan VTOL UAVs in Crosswind Turbulence" AHS 4th Decennial Specialist's Conference on Aeromechanics, Jan 21-23, 2004.
- [3] Akturk, A., Camci, C., "Double Ducted Fan as a Novel Ducted Fan Inlet Lip Separation Control Device" Proceedings of the International Powered Lift Conference, Philadelphia, PA, October 2010.
- [4] Camci, C. and Akturk, A., "Double-Ducted Fan" U.S. Patent No: US 8,821,123 B2, September 2014.
- [5] Akturk, A. and Camci, C., "Lip Separation and Inlet Flow Distortion Control in Ducted Fans Used in VTOL Systems," ASME paper GT2014-26249, ASME Turbo Expo 2014, June 2014.
- [6] Camci, C. and Akturk, A., "A VTOL-UAV Inlet Flow Distortion Reduction Concept using a New Flow Control Approach: Double-Ducted-Fan (DDF)," Proceedings of the ISROMAC 2016, International Symposium on Transport Phenomena and Dynamics of Rotating Machinery, Hawaii, Honolulu, April 2016.
- [7] Yarusevych, S., Sullivan, P.E., Kawall, J.G., "Smoke-Wire Flow Visualization in Separated Flows at Relatively High Velocities", AIAA Journal, Vol.47, No. 6, pp. 1592-1595, June 2009.
- [8] Sieverding, C.H., Bosche, P.V.D., "The use of Coloured Smoke to Visualize Secondary Flows in a Turbine-Blade Cascade", Journal of Fluid Mechanics, Vol. 134, pp. 85-89,1983.